International Journal of Smart Grid and Clean Energy

Magnetic field comparison of 6/4 and 8/6 switched reluctance motor by using the 3-D finite element method

S. Son-in, T. Kulworawanichpong, P. Pao-la-or *

School of Electrical Engineering, Suranaree University of Technology, Nakhonratchasima, Thailand

Abstract

Magnetic field is a crucial point for studying the behavior of switched reluctance motor (SRM) of electric vehicle (EV). Nowadays the pollution of the environment is increasing, which one of the problems is air pollution from vehicles. Hence, to reduce air pollution, EVs are another option. This paper presents a mathematical model of SRM, and it is confirmed the validity by using the three-dimensional finite element method (3-D FEM), which has developed in MATLAB. 3-D FEM is being used to determine magnetic field distribution in and around the SRMs. Moreover, this paper discusses the distribution of the magnetic field acting on the stator teeth around the air-gap. The simulation results compare for two types of three-phase 6/4 poles SRM and four-phase 8/6 poles SRM.

Keywords: Switched reluctance motor (SRM), 3-D finite element method (3-D FEM), electrical vehicle (EV), magnetic field, radial force

1. Introduction

In the 21st century, conventional vehicles produce air pollution has caused damage in term of the environment. The most significant air pollutants are from traditional vehicles [1]. Recently, EVs saw a resurgence due to EVs have few direct emission, technological developments, and an increased focus on renewable energy, thus rise attention to the EVs. The SRMs are becoming attractive for EVs propulsion in several decades, which definite advantages of simple, robust, heat tolerance and low-cost structure [2-4], especially the absence of copper windings or permanent magnets (PMs) and doubly salient structure in the rotor [5, 6]. There are much possible topological structures for SRM, mainly depending on the number of phases as well as the number of stator and rotor poles. Two basic SRMs are the three-phase 6/4 poles SRM, which has six stator poles and four rotor poles and the four-phase 8/6 poles SRM, which has eight stator poles and six rotor poles. The three-phase 6/4 poles SRM has the advantages of lower cost and high-speed operation. On the other hand, the four-phase 8/6 poles SRM has better starting torque and lower torque ripple.

The determination of numerical based on finite element method (FEM) analysis. The FEM is probably the most widely used mathematical approximation technique for solving electromagnetic problems, temperature rise, and heat transfer problem. The FEM is similar to the finite difference (FD) method, which the FEM is more efficient than the FD method due to flexibility, accuracy and it can gain a definite advantage when it applied in the SRM. This paper has considered the problem in three dimensions. Therefore 3-D FEM has been built to predict their performance.

2. Modeling of Magnetic Field for Switched Reluctance Motor

2.1. Numerical analysis

Regarding calculation, which electromagnetic problems mostly differential equation starting from the

*Manuscript received November 27, 2018; revised October 25, 2019.
Corresponding author: Tel.:+66-44-22-4400; *email*: padej@sut.ac.th
doi: 10.12720/sgce.9.1.33-43

magnetic vector potential equations in x, y and z direction for SRM from as follow (1), [7].

$$\frac{\partial}{\partial x}\left(\gamma\frac{\partial A}{\partial x}\right)+\frac{\partial}{\partial y}\left(\gamma\frac{\partial A}{\partial y}\right)+\frac{\partial}{\partial z}\left(\gamma\frac{\partial A}{\partial z}\right)+J_0=0 \tag{1}$$

where, A is the magnetic vector potential (Wb/m), γ is the magnetic reluctivity, which $\gamma=\frac{1}{\mu}$ by μ is magnetic permeability (H/m), and J_0 is the electrical current density (A/m^2).

2.2. Discretization

This paper compared with the 6/4 poles SRM and the 8/6 poles SRM. The three-phase 6/4 poles SRM structure consists of a magnetically dependent stator and rotor set, where each stator set includes six poles having 30 degrees arc length with coils wrapped around them while the rotor comprises of four poles with different arc lengths. The four-phase 8/6 poles SRM structure consists of a magnetically dependent stator and rotor set, where each stator set includes eight poles having 30 degrees arc length with coils wrapped around them while the rotor comprises of six poles with different arc lengths.

The motor configurations used in this study shown Table 1. [8], which refers to the SRM scaling of dimension as follows Fig. 1.-Fig. 3. Both tested specimens of SRMs have 72 mm of stator core outer diameter, 62 mm of stator core inner diameter and 35 mm of each module thickness. Applying the 3-D FEM for solving the PDE can be discretized by using linear tetrahedron elements and accomplished by using 3-D grid generation. The three-phase 6/4 poles SRM consists of 51,460 nodes and 298,580 elements. The four-phase 8/6 poles SRM consists of 41,134 nodes and 236,228 elements.

Due to the precise comparison between the three-phase 6/4 poles SRM and the four-phase 8/6 poles SRM, the mesh densities are considered to be precisely the same for both cases [9]. The model with mesh densities used in the simulation is as shown in Fig. 3. If the conduction currents flow in one of the phases, as shown in Fig. 2. [10], then electromagnetic forces will be produced between the rotor and stator poles.

Table 1. The motor specifications

Parameter	Value	Parameter	Value
Stator core outer diameter	72 mm	Stator core inner diameter	62 mm
Stator pole arc	30 degree	Air gap	0.25 mm
Rotor pole arc	45 degree	Rotor shaft diameter	10 mm
Each module thickness	35 mm	Rotor core outer diameter	41.5 mm

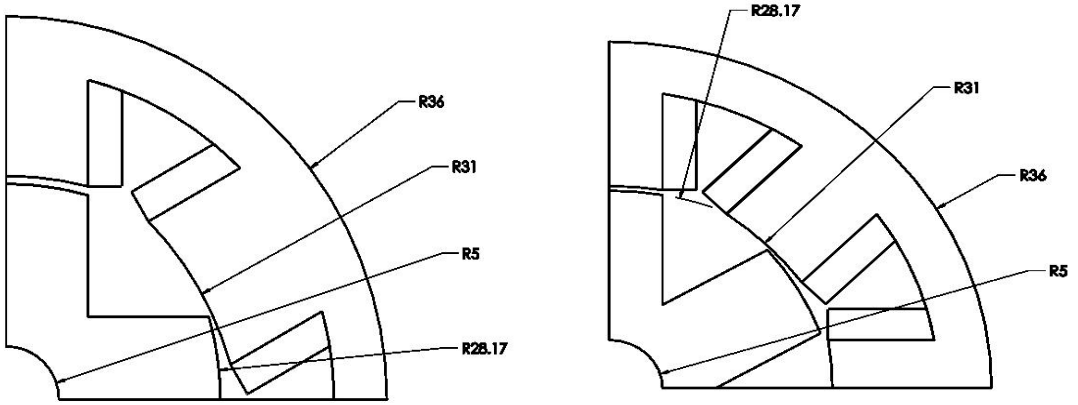

(a) (b)

Fig .1. The geometry of the tested SRM with dimension (mm) (a) the 6/4 poles SRM (b) the 8/6 poles SRM

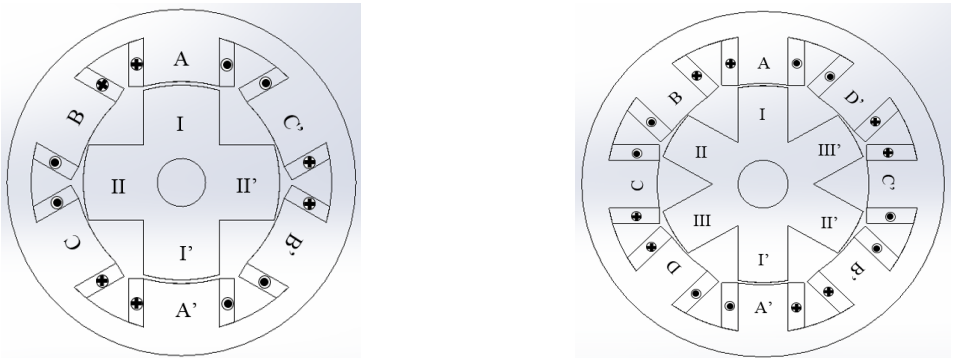

(a) (b)

Fig .2. Detail of the winding distribution (a) three-phase in 6 slots (b) four-phase in 8 slots

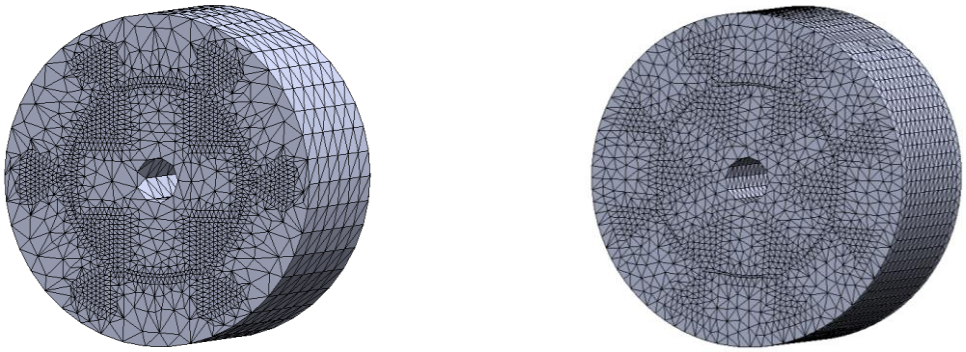

(a) (b)

Fig .3. Discretization (a) the 6/4 poles SRM (b) the 8/6 poles SRM

2.3. 3-D FEM formulation

Interpolate function of each element was derived by using the Galerkin approach, which is the exact weight residual technique for which the weighting functions are similar to the shape functions. The shape function for 3-D FEM used in this research is the application of three dimensions (4 nodes tetrahedron element). According to this method, the magnetic vector potential expressed as follow (2), [11]

$$A(x,y,z) = A_i N_i + A_j N_j + A_k N_k + A_l N_l \tag{2}$$

where, N_i, N_j, N_k, N_l are the element shape functions of node i, j, k, l respectively and A_i, A_j, A_k, A_l are the approximation of the magnetic vector potential at each node i, j, k, l respectively. The weighting functions are similar to the shape function, which is

$$N_n = \frac{a_n + b_n x + c_n y + d_n z}{6V} \tag{3}$$

where, $n = i, j, k, l$ and V is the volume of the tetrahedron element, which expressed as

$$V = \frac{1}{6}\begin{vmatrix} 1 & x_i & y_i & z_i \\ 1 & x_j & y_j & z_j \\ 1 & x_k & y_k & z_k \\ 1 & x_l & y_l & z_l \end{vmatrix} \tag{4}$$

And the positional coefficient defined by

$$a_i = x_l\left(y_j z_k - y_k z_j\right) + x_k\left(y_l z_j - y_j z_l\right) + x_j\left(y_k z_l - y_l z_k\right) \quad b_i = y_l\left(z_k - z_j\right) + y_k\left(z_j - z_l\right) + y_j\left(z_l - z_k\right)$$
$$a_j = x_l\left(y_k z_i - y_i z_k\right) + x_k\left(y_i z_l - y_l z_i\right) + x_i\left(y_l z_k - y_k z_l\right) \quad b_j = y_l\left(z_i - z_k\right) + y_i\left(z_k - z_l\right) + y_k\left(z_l - z_i\right)$$
$$a_k = x_l\left(y_i z_j - y_j z_i\right) + x_j\left(y_i z_i - y_i z_l\right) + x_i\left(y_j z_l - y_l z_j\right) \quad b_k = y_l\left(z_j - z_i\right) + y_j\left(z_i - z_l\right) + y_i\left(z_l - z_j\right)$$
$$a_l = x_k\left(y_j z_i - y_i z_j\right) + x_j\left(y_i z_k - y_k z_i\right) + x_i\left(y_k z_j - y_j z_k\right) \quad b_l = y_k\left(z_i - z_j\right) + y_i\left(z_j - z_k\right) + y_j\left(z_k - z_i\right)$$
$$c_i = x_l\left(z_j - z_k\right) + x_j\left(z_k - z_l\right) + x_k\left(z_l - z_j\right) \quad d_i = x_l\left(y_k - y_j\right) + x_k\left(y_j - y_l\right) + x_j\left(y_l - y_k\right)$$
$$c_j = x_l\left(z_k - z_i\right) + x_k\left(z_i - z_l\right) + x_i\left(z_l - z_k\right) \quad d_j = x_l\left(y_i - y_k\right) + x_i\left(y_k - y_l\right) + x_k\left(y_l - y_i\right)$$
$$c_k = x_l\left(z_i - z_j\right) + x_i\left(z_j - z_l\right) + x_j\left(z_l - z_i\right) \quad d_k = x_l\left(y_j - y_i\right) + x_j\left(y_i - y_l\right) + x_i\left(y_l - y_j\right)$$
$$c_l = x_k\left(z_j - z_i\right) + x_j\left(z_i - z_k\right) + x_i\left(z_k - z_j\right) \quad d_l = x_k\left(y_i - y_j\right) + x_i\left(y_j - y_k\right) + x_j\left(y_k - y_i\right)$$

Formulating each element equations of (1) and substituting the approximate results in (1), which is equal residual function as follow (5).

$$\frac{\partial}{\partial x}\left(\gamma\frac{\partial A}{\partial x}\right) + \frac{\partial}{\partial y}\left(\gamma\frac{\partial A}{\partial y}\right) + \frac{\partial}{\partial z}\left(\gamma\frac{\partial A}{\partial z}\right) + J_0 = R \tag{5}$$

where, R is the residual function. The method of the weighted residual with Galerkin approach applied to the PDE, where the integrations performed over the element domain V expresses as

$$\int_V \left(N_n\left[\frac{\partial}{\partial x}\left(\gamma\frac{\partial A}{\partial x}\right) + \frac{\partial}{\partial y}\left(\gamma\frac{\partial A}{\partial y}\right) + \frac{\partial}{\partial z}\left(\gamma\frac{\partial A}{\partial z}\right)\right] + J_0 \right) dV = 0$$

Which the equation can was written in term of the matrix as form (6).

$$[K]\{A\} = \{F\} \tag{6}$$

where, [K] is the permeability matrix of the problem and for one element consists of 4 nodes, expression of the FEM approximation is 4×4 a matrix, which shown in term of positional coefficient as follow (7).

$$[K]_{4x4} = \frac{\gamma}{36V}\begin{bmatrix} b_1b_1+c_1c_1+d_1d_1 & b_1b_2+c_1c_2+d_1d_2 & b_1b_3+c_1c_3+d_1d_3 & b_1b_4+c_1c_4+d_1d_4 \\ b_1b_2+c_1c_2+d_1d_2 & b_2b_2+c_2c_2+d_2d_2 & b_2b_3+c_2c_3+d_2d_3 & b_2b_4+c_2c_4+d_2d_4 \\ b_1b_3+c_1c_3+d_1d_3 & b_2b_3+c_2c_3+d_2d_3 & b_3b_3+c_3c_3+d_3d_3 & b_3b_4+c_3c_4+d_3d_4 \\ b_1b_4+c_1c_4+d_1d_4 & b_2b_4+c_2c_4+d_2d_4 & b_3b_4+c_3c_4+d_3d_4 & b_4b_4+c_4c_4+d_4d_4 \end{bmatrix} \tag{7}$$

where {F} is the load vector of a problem as follow (8).

$$\{F\}_{4\times1} = \frac{-J_0V}{4}\begin{bmatrix}1\\1\\1\\1\end{bmatrix} \tag{8}$$

The electrical current density (J_0) determines from the current through the area of conductors can define by (9), where N is turn number of the conductor $(turn)$, I is current quantities (A), and A is an area of conductors (m^2).

$$J_0 = \frac{N\times I}{A} \tag{9}$$

3. Calculating Current and Speed of SRM

SIMULINK is a block diagram for simulation and model-based design. It supports the system-level design, simulation, automatic code generation, and continuous test. SIMULINK provides a graphical editor, customizable block libraries and solving for modeling and simulating dynamics system [12].

Both current (I) of the 6/4 poles SRM, three-phase, 60 kW, and the 8/6 poles SRM, four-phase, 75 kW from SIMULINK fed to SRMs model as follow Fig.4.(a) and Fig.4.(b), respectively are shown each phase of SRMs currently, and both angular velocity (rad/s) of the 6/4 poles SRM and the 8/6 poles SRM as follow Fig.5.(a) and Fig.5.(b), respectively are shown speed each SRMs. In this study the simulation in no-load condition $(T_L = 0)$.

From SIMULINK result, starter current and steady-state current of the 6/4 poles SRM are higher than starter current and steady-state current of the 8/6 poles SRM, which both can also observe the value of starter current and steady-state flow has a positive value and few negative values of current. The speed operation of 6/4 poles SRM is higher than 8/6 poles SRM, which relate to the number of stators.

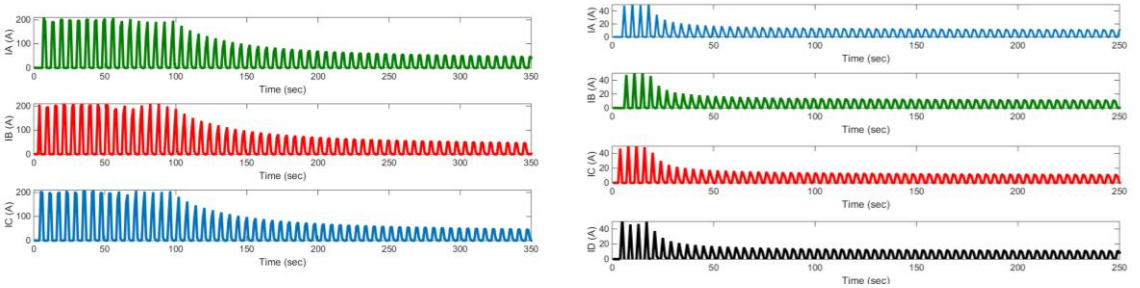

(a) (b)

Fig. 4. Starter current and steady-state current for (a) the 6/4 poles SRM (b) the 8/6 poles SRM

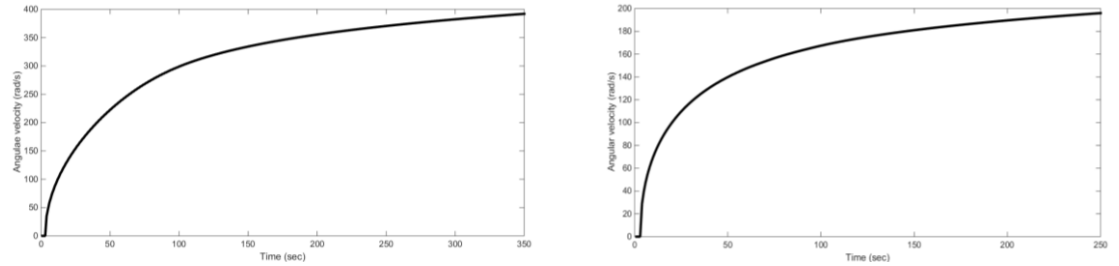

(a) (b)

Fig. 5. The angular velocity of (a) the 6/4 poles SRM (b) the 8/6 poles SRM

4. 3-D FEM Simulation Result

The simulation of 3-D FEM written by MATLAB programming. The Dirichlet boundary condition $(A = 0)$ is specified both along the outer surface of the stator core and along the inner surface rotor core of the 6/4 poles SRM and the 8/6 poles SRM. In the SIMULINK result, both current and speed used to solving the FEM equation. The size of each time step is the time needed for the rotor turn fixed at $\Delta\theta = (360/4)°$ of the 6/4 poles SRM, which 4 is a number of rotor slot and $\Delta\theta = (360/6)°$ of the 8/6 poles SRM, which 6 is a number of rotor slot. the ratio of The specific medium permeability (μ) is related the relative permeability of the stator and rotor core (μ_r) and the free space permeability (μ_0) by $\mu = \mu_0 \times \mu_r$, where $\mu_r = 5000$, and $\mu_0 = 4\pi \times 10^{-7} H/m$ [13-15].

For 3-D FEM simulation result can be presented by graphically in the filled polygon of magnetic vector potential and the magnetic field dispersed of SRM. Fig.6.(a) and Fig.7.(a) shown the magnetic vector potential distribution in 3-D of the 6/4 poles SRM and the 8/6 poles SRM, respectively. Fig.6.(b)-Fig.6.(d) shown the cross-sectional magnetic vector potential distribution of the 6/4 poles SRM at 0, 30 and 60 degrees in the aligned position, respectively (repeat every 90 degrees). Fig.7.(b)-Fig.7.(e) shown the cross-sectional magnetic vector potential distribution of the 8/6 poles SRM at 0, 15, 30 and 45 degrees, respectively (repeat every 60 degrees). To be consistent, Fig.8.(a) and Fig.9.(a) shown the magnetic field distribution of the SRMs in 3-D of the 6/4 poles SRM and the 8/6 poles SRM, respectively. Fig.8.(b)-

Fig.8.(d) shown the cross-sectional magnetic field distribution of the 6/4 poles SRM at 0, 30 and 60 degrees of the rotor position, respectively. Fig.9.(b)-Fig.9.(e) shown the cross-sectional magnetic field distribution of the 8/6 poles SRM at 0, 15, 30 and 45 degrees in the aligned position, respectively.

From 3-D FEM simulation result can also observe that the magnetic vector potential and the magnetic field distribution between the 6/4 poles SRM and the 8/6 poles SRM are different. The value of the magnetic vector potential of the 6/4 poles SRM is higher than the 8/6 poles SRM. The amount of a magnetic field of the 6/4 poles SRM is higher than the 8/6 poles SRM, which the magnetic field related with the magnetic vector potential to $B = \nabla \times A$. Meanwhile, the lowest magnetic field occurs at all stator slot, and the area of the coil is fed each phase of SRMs currently because the magnetic field is a vector field that describes the magnetic influence of electrical currents and magnetized materials. The value of the magnetic field has an area of the stator and rotor cores because it has the high relative permeability. The relative permeability is the measure of the ability of a material of a magnetic field. The highest magnetic field occurs at stator and rotor teeth.

The value of magnetic field (B) inside each element is obtained from $B = \nabla \times A$, which magnetic field (B) has a component in x and y direction [16] computed by (10)-(11)

$$B_x = \frac{\partial A_z}{\partial y} = \frac{c_i A_i + c_j A_j + c_k A_k + c_l A_l}{6V} \tag{10}$$

$$B_y = -\frac{\partial A_z}{\partial x} = -\left(\frac{b_i A_i + b_j A_j + b_k A_k + b_l A_l}{6V} \right) \tag{11}$$

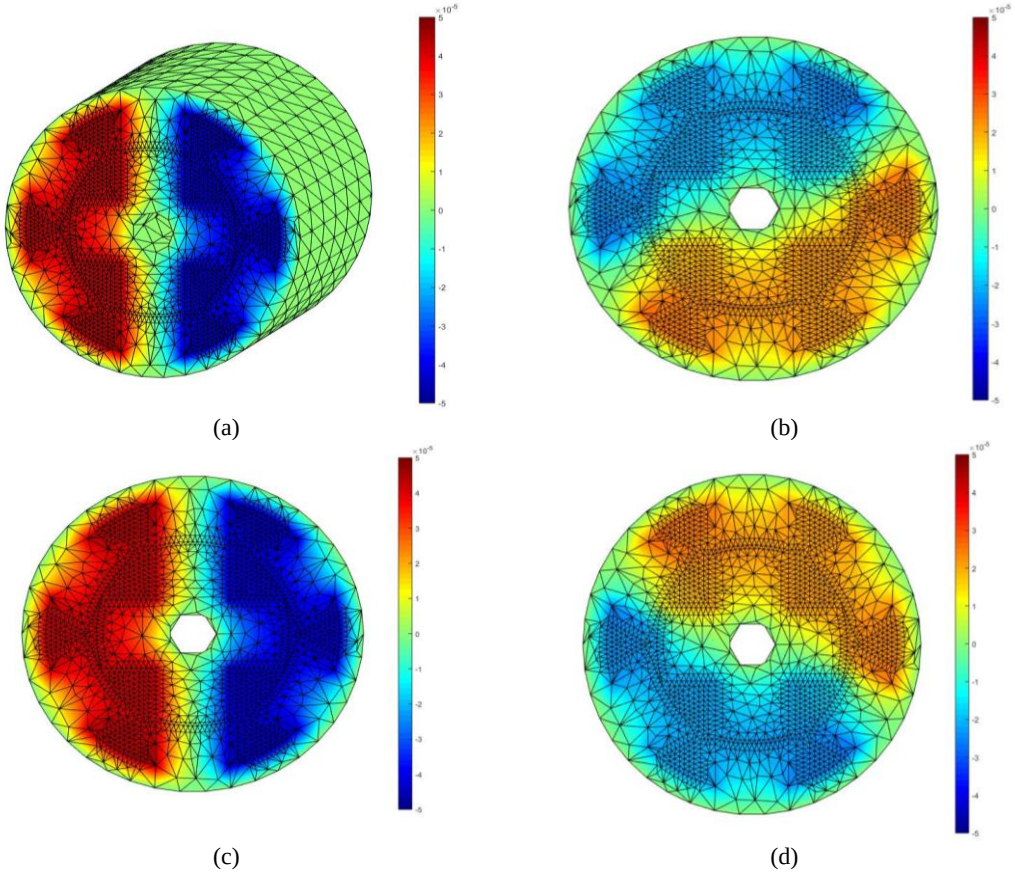

(a) (b)

(c) (d)

Fig.6. Magnetic vector potential distribution (Wb/m) of the 6/4 poles SRM (a) example at the rotor position $30°$ in 3-D (b) at the rotor position $0°$ (c) at the rotor position $30°$ (d) at the rotor position $60°$

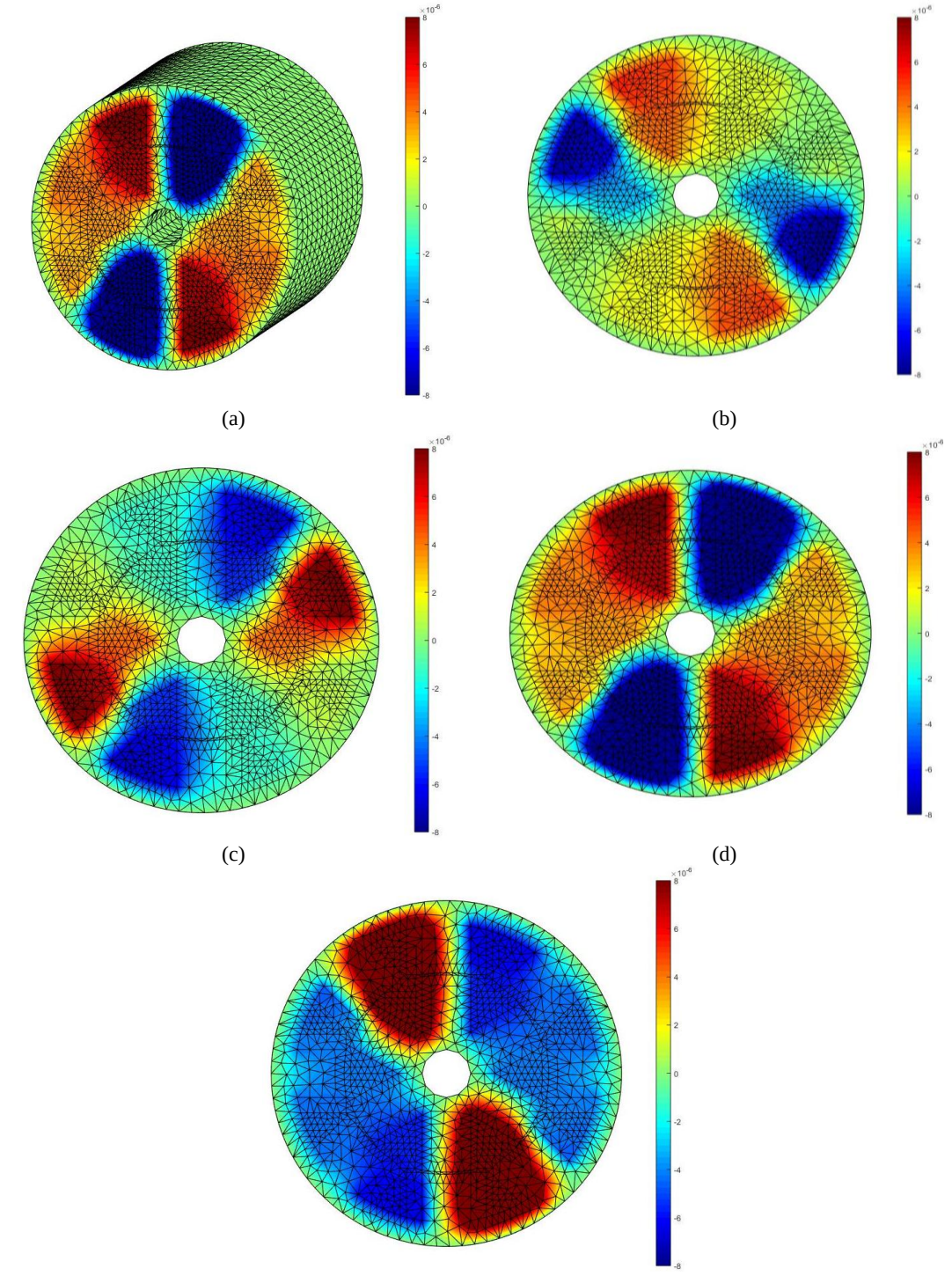

Fig.7. Magnetic vector potential distribution (Wb/m) of the 8/6 poles SRM (a) example at the rotor position $30°$ in 3-D (b) at the rotor position $0°$ (c) at the rotor position $15°$ (d) at the rotor position $30°$ (e) at the rotor position $45°$

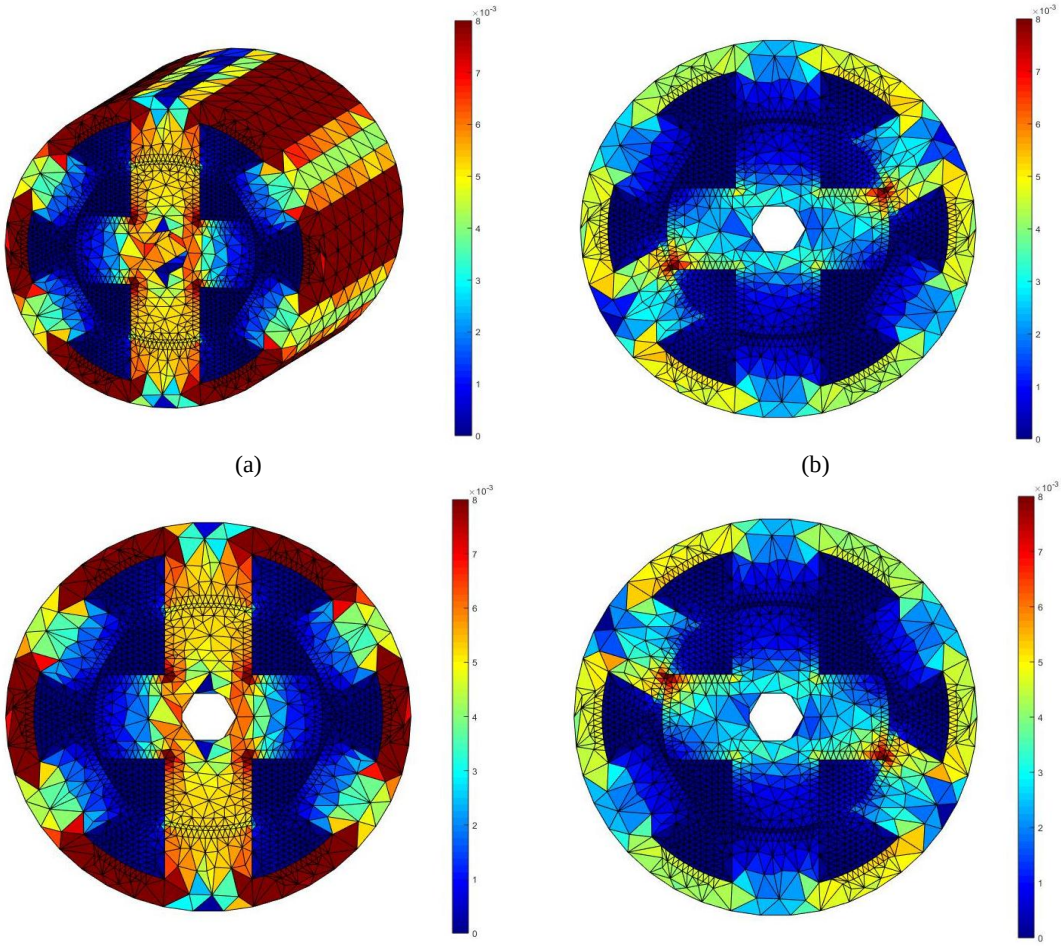

(a) (b)

(c) (d)

Fig.8. Magnetic field distribution (T) of the 6/4 poles SRM (a) example at the rotor position $30°$ in 3-D (b) at the rotor position $0°$ (c) at the rotor position $30°$ (d) at the rotor position $60°$

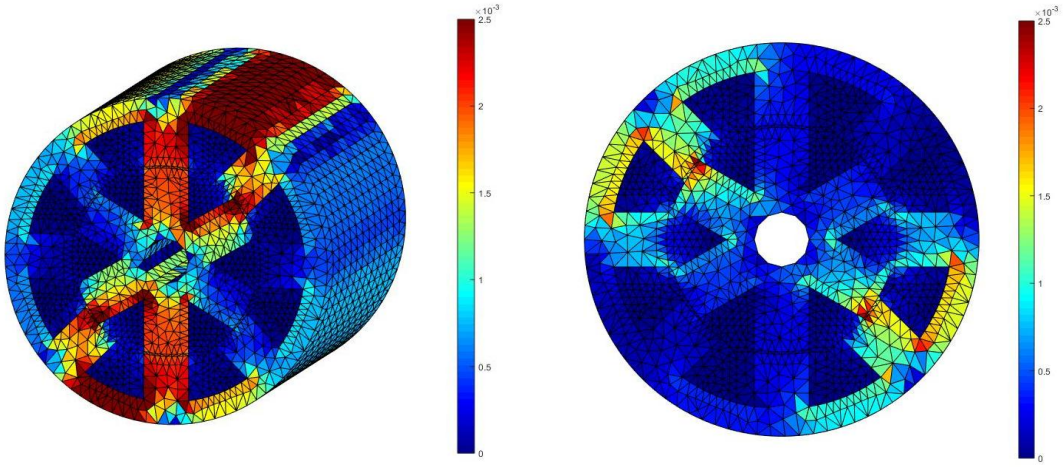

(a) (b)

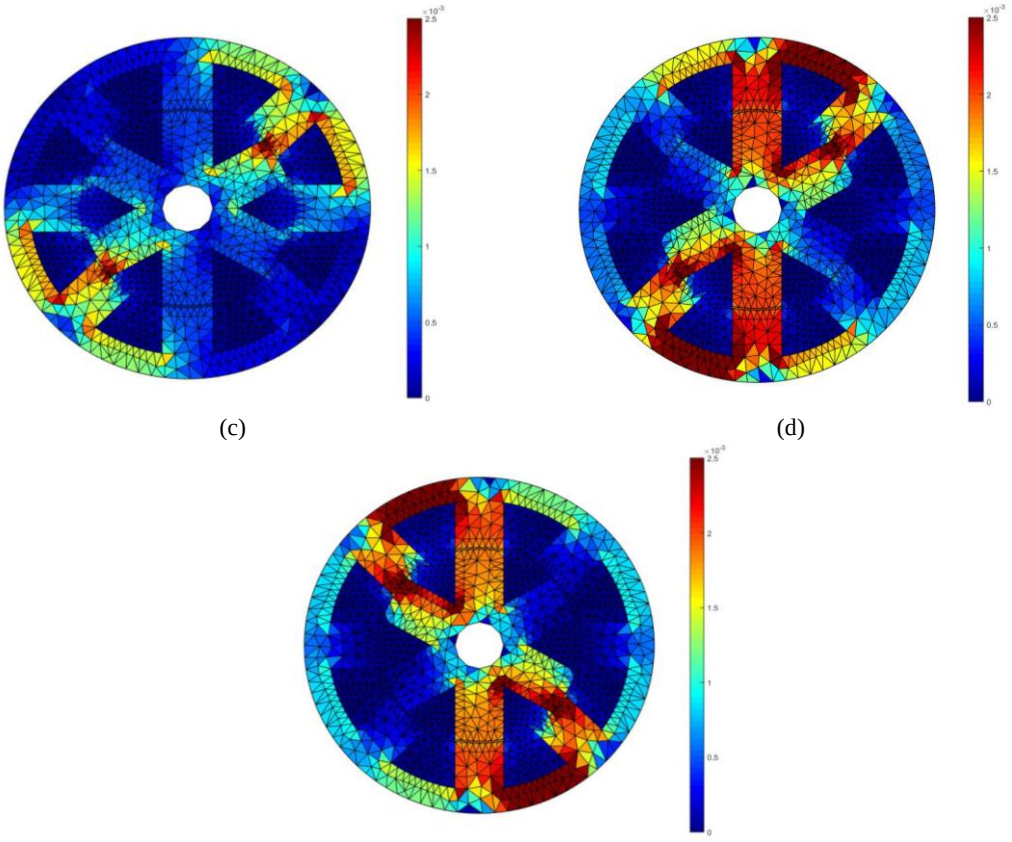

(c) (d)

(e)

Fig.9. Magnetic field distribution (T) of the 8/6 poles SRM (a) example at the rotor position $30°$ in 3-D (b) at the rotor position $0°$ (c) at the rotor position $15°$ (d) at the rotor position $30°$ (e) at the rotor position $45°$

Moreover, the radial flux density (B_r) and tangential flux density (B_t) acting on the air-gap can be expressed in cylindrical coordinate as a function of B_x and B_y, which is

$$B_r = B_x \cos\phi + B_y \sin\phi \tag{12}$$

$$B_t = -B_x \sin\phi + B_y \cos\phi \tag{13}$$

where, ϕ is the angle of stator teeth center concerning the positively horizontal axis.

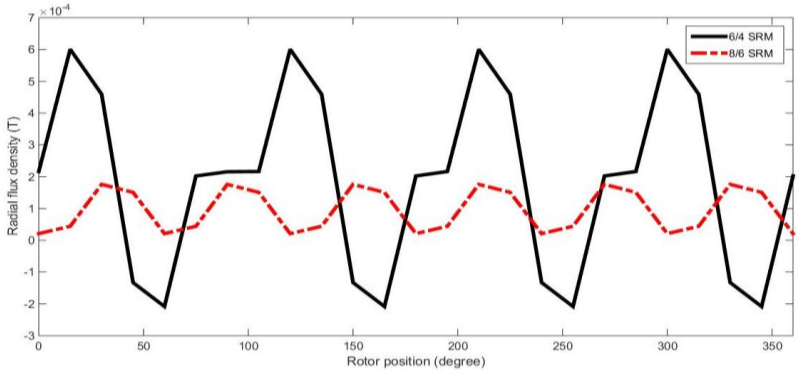

Fig.10. Compare of the radial flux density between the 6/4 poles SRM and the 8/6 poles SRM

From Fig.10. is shown the radial flux density acting on the one stator tooth in the radial direction between the three-phase 6/4 poles SRM and the four-phase 8/6 poles SRM. It can also observed that the curve in Fig.10. resembles a sinusoid. Maxwell's stress equation used to determine the distribution of the radial force across the air-gap as from [17],

$$F_r = \frac{1}{2\mu_0}\left(B_r^2 - B_t^2\right) \tag{14}$$

The 3-D FEM approach is also utilized to calculate the SRM's vibration. For our computational vibration is considered the stator teeth, by assuming that the force acting on the center of stator teeth could was transmitted through to the SRM frame.

The radial force $\left(F_r\right)$ generally means a force exerted in a radial direction towards the center and affected the stator radial vibration and acoustic noise in SRMs [18]. The curvature of the radial flux density of the 8/6 pole SRM is smoother than the 6/4 poles SRM. The amplitude of 6/4 poles SRM is higher than 8/6 poles SRM. If there is nothing to disturb, less the radial force into the slot, in this case, to cause less vibration, compare the 6/4 poles SRM is vibrated than the 8/6 poles SRM.

5. Conclusion

This paper describes the modeling and simulation technique via the three-dimensional finite element method (3-D FEM) for solving the partial differential equation of magnetic vector potential, which written in MATLAB programming. Also, the simulated result present in this paper shows that 3-D FEM can be used to study of the magnetic vector potential and the magnetic field distribution in and around the switched reluctance motor (SRM) by comparison between the three-phase 6/4 poles SRM and the four-phase 8/6 poles SRM. Due to the results show this method is simple to illustrate how the magnetic vector potential and the magnetic field throughout the volume of SRMs. This advantage can be developed to calculate based on the magnetic field, e.g., magnetic vibration and acoustic noise.

Conflict of Interest

The authors declare no conflict of interest.

Author Contributions

Pao-la-or conducted the research; Son-in and Kulworawanichpong analyzed the data; Son-in and Pao-la-or wrote the paper; all authors had approved the final version.

Acknowledgements

The School of Electrical Engineering supported this work, Institute of Engineering, Suranaree University of Technology.

References

[1] Pindoriya RM, Rajpurohit S, Kumar R, Srivastava K. Comparative analysis of permanent magnet motors and switched reluctance motors capabilities for electric and hybrid electric vehicles, in *IEEMA Engineer Infinite Conference*, 2018.

[2] Mir S, Husain I, Elbuluk M. Switched reluctance motor modeling with on-line parameter identification. *IEEE Transactions on Industry Applications*, 1998.

[3] Chen H, Yan W, Gu JJ, Sun M. Multiobjective optimization design of a switched reluctance motor for low-speed electric vehicles with a Taguchi–CSO algorithm. *IEEE/ASME Transactions on Mechatronics*, 2018.

[4] Rajkumar S, Sedhuraman K., Purimetla S, Joycy FLA. Design and analysis of high speed switched reluctance motor for two different materials. presented at the National Level Technical Conference, March 1, 2015.

[5] Singh G, Singh B. Control of a 12/8 switched reluctance motor with saturation characteristics for light electric vehicle. *IEEMA Engineer Infinite Conference (eTechNxT)*, 2018.

[6] Sholahuddin U, Purwadi A, Heryana N, Rizqiawan A, Haroen Y. Magnetic simulation comparation of 30 kW switched reluctance motor with 6/4 and 6/10 design configurations for electric vehicle. *International Conference on Electrical Engineering and Computer Science (ICEECS)*, Indonesia, 2014.

[7] Siadatan A, Najmi V, Asgar M, Afjei E. A new 6/4 two layers switched reluctance motor: Concept, simulation and analysis," in *International Aegean Conference on Electrical Machines and Power Electronics and Electromotion, Joint Conference*, Turkey, 2011.

[8] Siadatan A, Asgar M, Naimi V, Afjei E. A novel method for torque ripple reduction in 6/4 two rotor stack switched reluctance motor.

[9] Torkaman H, Afjei E. Magnetio static field analysis regarding the effects of dynamic eccentricity in switched reluctance motor. *Progress In Electromagnetics Research M*, 2009.

[10] Nezamabadi MM, Afjei E, Naemi MR, Afjai AA. Design and 3D-FEM analysis of a rotary – linear switched reluctance motor, presented at the International Symposium on Power Electronics, Electrical Drives, Automation and Motion, 2016.

[11] Pao-la-or P, Isaramongkolrak A, and Kulworawanichpong T. Finite element analysis of magnetic field distribution for 500- kV power transmission system. *Engineering Letters, No.1*, 2010;18: 1-9.

[12] Zhang J, Wang L, Zhang H, & Gao R. Non-linear radial force simulation of switched reluctance motors based on finite element model. *IEEE International Conference on Robotics and Biomimetics*, 2009.

[13] Pao-la-or P, Peaiyoung S, Kulworawanichpong T, and Sujitjorn S. Effect of the geometry of the rotor slot on the mechanical vibration of three-phase induction motors, present at the 7th WSEAS International conference on simulation, modeling, and optimization, Beijing, China, Septemper 15-17, 2007.

[14] Parreira B, Rafael S, Pires S, Branco PC. (n.d.), Obtaining the magnetic characteristics of an 8/6-switched reluctance machine: FEM analysis and experimental tests. *IEEE International Symposium on Industrial Electronics*, 2005.

[15] Afjai E, Seyadatan A, Torkaman H. A new two-phase bidirectional hybrid switched reluctance motor field-assisted generator. *Journal of Applied Sciences*, 9(4): 765-770. Available: https://www.researchgate.net/publication/46029750

[16] Bedrosian G. (n.d.). A new method for coupling finite element field an efficient technique for solving the coupled finite solutions with external circuits and kinematics element and circuit equations. in *Digest of the Fifth Biennial IEEE Conference on Electromagnetic Field Computation*, 1993.

[17] Li J, Song X, Cho Y. Comparison of 12/8 and 6/4 switched reluctance motor: Noise and vibration aspects. *IEEE Transactions on Magnetics*, 2008.

[18] Jun ZH, Gao C., Wang H. Analysis of radial force for switched reluctance motor. in *International Conference on Applied Superconductivity and Electromagnetic Device, Beijing, China*, 2013.